Arch. Metall. Mater., Vol. 61 (2016), No 2, p. 587–592

DOI: 10.1515/amm-2016-0100

J. ROMANOWSKA*#, B. WIERZBA*, J. MARKOWSKI**, M. ZAGULA-YAVORSKA*, J. SIENIAWSKI*

THE Ni-Al-Hf MULTIPHASE DIFFUSION

The generalized Darken method was applied to simulate the diffusion between γ-Ni| γ'-Ni_3Al and γ'-Ni_3Al|β-NiAl interfaces. The results of calculations were compared with the experimental concentration's profiles of nickel, aluminum and hafnium in aluminide and hafnium doped aluminide coatings deposited by the CVD and PVD methods on pure nickel. The method deals with the Wagner's integral diffusion coefficients and thermodynamic data - activities of components. The experimental results agree with the simulated ones.

Keywords: NiAlHf system, reactive diffusion, simulation, aluminide coatings

1. Introduction

Aluminide coatings are essential in many high temperature applications such as protecting turbine blades in the hot section of aerospace engines against oxidation and hot corrosion. Alloyed nickel aluminides are of particular interest as bond coats in thermal barrier coatings due to their high strength and abilities to form a protective aluminium oxide layer. This aluminium oxide layer limits the amount of oxygen that can diffuse into critical engine components causing catastrophic failure [1-3]. However, aluminide coatings do not fulfill the requirements of good adhesion and long oxidation resistance at high temperature. Therefore, in order to improve the oxidation resistance of the coating it is necessary to slow the oxide scale growth and improve the oxide adherence. The Al concentration gradient between the superalloy and the coating is the driving force of the Al loss. Candidate diffusion barrier materials should retard Al diffusion at high temperatures, possess good thermo-mechanical compatibility with the substrate and the coating and remain relatively stable for extended periods of time at high temperature. Some elements, for instance Pt, Pd, or RE (reactive) elements such as: Zr, Hf or Ir are known to enhance oxidation resistance [6-10]. Hf-rich precipitates segregate close to the coating surface, along grain boundaries and at the interface between the additive layer and the interdiffusion layer. This is due to the low hafnium solubility and low diffusivity in the aluminide coating. The interface corresponds to the initial surface of the substrate. Hf-rich particles at the interface indicate, that hafnium deposition occurs at the beginning of the vapour phase aluminizing process [11]. RE ions first segregate at the scale/alloy interface and then diffuse to the oxide scale surface along oxide grain boundaries toward the scale/gas interface under the oxygen potential gradient. The slow outward diffusion of large hafnium ions inhibits the outward diffusion of small Al ions and inward diffusion of oxygen. This modification of the transportation process from the simultaneous Al and O diffusion to the predominant oxygen outward diffusion is called a "blocking effect" and is supposed to be responsible for the reduction of the alumina scale growth rate [12,13]. Hafnium modified alumina coatings have the lowest oxide scale growth rate among the RE doped coatings. The hafnium ion has the largest effective radius of all RE ions, despite its smaller actual radius. As the real radius of RE ions reflects only the strength of physical blocking, an effective radius was introduced to reflect the strength of " blocking effect" of RE ions in the outward Al diffusion [13-15]. Hafnium can be introduced to the alloy or to the coating in the CVD or pack cementation processes [16-17].

This paper presents results of the simulation of three kinds of aluminide coatings: the undoped one and two kinds of hafnium doped ones. In the first case a 3 mm thick hafnium layer was deposited by the PVD method and then, the aluminide layer was deposited by the CVD method. In the second case hafnium was co-deposited with aluminum in the CVD process. The influence of hafnium ions on the aluminide coating's growth on pure nickel is analyzed by means of the instrinct diffusion. The experimental results are compared with the calculated ones.

2. Model

The aluminide coatings deposited on nickel and nickel superalloys consist of three layers. The top layer consists of the β-NiAl phase, the second zone, below consists of the γ'-Ni_3Al and the γ-Ni(Al) phase is located underneath [18,19]. In this paper the diffusion between γ-Ni| γ'-Ni_3Al and γ'-Ni_3Al|β-NiAl interfaces is calculated. We assume that both γ'-Ni_3Al and β-NiAl phases have just been formed by nucleation (have constant thickness ~ 1 nm) and now they grow between pure Ni and Al.

* RZESZÓW UNIVERSITY OF TECHNOLOGY, DEPARTMENT OF MATERIALS SCIENCE, 2 W. POLA STR., 35-959 RZESZÓW, POLAND

** WROCŁAW UNIVERSITY OF TECHNOLOGY, FACULTY OF ELECTRONICS, 11/17 Z. JANISZEWSKIEGO STR., 50-372 WROCŁAW, POLAND

Corresponding author: jroman@prz.edu.pl

As to describe the fluxes of Ni atoms through both intermetallic phases, the Wagner's expression can be applied:

$$\Omega J_B^{(\alpha)} = -\tilde{D}^{(\alpha)} \nabla N_B^{(\alpha)} \equiv -\tilde{D}^{(\alpha)} \nabla N_B^{(\alpha)} \frac{\int_{X_{j+1}}^{X_j} dx}{\int_{X_{j+1}}^{X_j} dx} = -\frac{\int_{X_{j+1}}^{X_j} \tilde{D}^{(\alpha)} \nabla N_B^{(\alpha)} dx}{\int_{X_{j+1}}^{X_j} dx} = -\frac{\int_{N_B^{(\alpha)}(L)}^{N_B^{(\alpha)}(R)} \tilde{D}^{(\alpha)} dN}{X_{j+1} - X_j} \tag{1}$$

where the term $\int_{N_B^{(\alpha)}(L)}^{N_B^{(\alpha)}(R)} \tilde{D}^{(\alpha)} dN$ is called the Wagner's integral diffusion coefficient [20] and is expressed as:

$$\int_{N_B^{(\alpha)}(L)}^{N_B^{(\alpha)}(R)} \tilde{D}^{(\alpha)} dN = \tilde{D}^{(\alpha)} \Delta N_B^{(\alpha)} \tag{2}$$

It is an effective diffusion coefficient averaged over the phase. Wagner's integral coefficient can be transformed using Darken relation expressing the interdiffusion coefficient by the intrinsic diffusion coefficients and second derivative of the Gibbs potential $\left(\frac{\partial^2 g^{(\alpha)}}{\partial N_B^{(\alpha)2}} \equiv g''^{(\alpha)} \right)$:

$$\tilde{D}^{(\alpha)} = \left(N_B^{(\alpha)} D_A^{(\alpha)} + N_A^{(\alpha)} D_B^{(\alpha)} \right) \frac{N_A^{(\alpha)} N_B^{(\alpha)}}{RT} \frac{\partial^2 g^{(\alpha)}}{\partial N_B^{(\alpha)2}} \tag{3}$$

In the binary system at the constant temperature and when stresses are negligible the integral and differential forms of the Gibbs relations are expressed by:

$$g^{(\alpha)} = N_A^{(\alpha)} \mu_A^{(\alpha)} + N_B^{(\alpha)} \mu_B^{(\alpha)} \tag{4}$$

$$\mathrm{d}g^{(\alpha)} = \mu_A^{(\alpha)} \mathrm{d}N_A^{(\alpha)} + \mu_B^{(\alpha)} \mathrm{d}N_B^{(\alpha)} = \left(\mu_B^{(\alpha)} - \mu_A^{(\alpha)} \right) \mathrm{d}N_B^{(\alpha)} \tag{5}$$

where $g^{(\alpha)}$ is the Gibbs free energy $\mu_A^{(\alpha)}$ and $\mu_B^{(\alpha)}$ denote the chemical potentials. The Gibbs and the chemical potentials are expressed per one atom, for example: $g^j = G^j / N_A$. It will be convenient here to use the following form of the differential Gibbs relation, Eq. :

$$g'^{(\alpha)} = \frac{\partial g^{(\alpha)}}{\partial N_B^{(\alpha)}} = \mu_B^{(\alpha)} - \mu_A^{(\alpha)}. \tag{6}$$

All quantities in Eqs. (4) - (6) depend on time and position.

Eq. (6) allows to calculate the dependence of the chemical potential on the molar ratio:

$$\frac{\partial \mu_B^{(\alpha)}}{\partial N_B^{(\alpha)}} = \frac{\partial^2 g^{(\alpha)}}{\partial \left(N_B^{(\alpha)} \right)^2} + \frac{\partial \mu_A^{(\alpha)}}{\partial N_B^{(\alpha)}} = g''^{(\alpha)} + \frac{\partial \mu_A^{(\alpha)}}{\partial N_B^{(\alpha)}}. \tag{7}$$

From the Gibbs Duheme relation $\left(N_A^{(\alpha)} \mathrm{d}\, \mu_A^{(\alpha)} = -N_B^{(\alpha)} \mathrm{d}\, \mu_B^{(\alpha)} \right)$ it follows the relation:

$$\frac{\partial \mu_A^{(\alpha)}}{\partial N_B^{(\alpha)}} = -\frac{N_B^{(\alpha)}}{N_A^{(\alpha)}} \frac{\partial \mu_B^{(\alpha)}}{\partial N_B^{(\alpha)}} \tag{8}$$

Combining (10) and (3) the composition dependence of the chemical potential is given by:

$$\left(1 + \frac{N_B^{(\alpha)}}{N_A^{(\alpha)}} \right) \frac{\partial \mu_B^{(\alpha)}}{\partial N_B^{(\alpha)}} = \frac{1}{N_A^{(\alpha)}} \frac{\partial \mu_B^{(\alpha)}}{\partial N_B^{(\alpha)}} = g''^{(\alpha)}. \tag{9}$$

From Eq. (9) the composition dependence of the chemical potentials equals:

$$\frac{\partial \mu_B^{(\alpha)}}{\partial N_B^{(\alpha)}} = N_A^{(\alpha)} g''^{(\alpha)} \quad \text{and} \quad \frac{\partial \mu_A^{(\alpha)}}{\partial N_A^{(\alpha)}} = N_B^{(\alpha)} g''^{(\alpha)} \tag{10}$$

Upon substituting (10) into (3) we have:

$$\tilde{D}^{(\alpha)} = \left(N_B^{(\alpha)} D_A^{(\alpha)} + N_A^{(\alpha)} D_B^{(\alpha)} \right) \frac{N_B^{(\alpha)}}{RT} \frac{\partial \mu_B^{(\alpha)}}{\partial N_B^{(\alpha)}} \tag{11}$$

Both interfaces γ'-Ni_3Al and β-NiAl will shift according to the following growth laws:

$$\begin{aligned} \left(1 - N_B^{(\gamma')} \right) \frac{\mathrm{d}X^{\gamma|\gamma'}}{\mathrm{d}t} &= 0 - \frac{\tilde{D}^{(\gamma')} \Delta N_B^{(\gamma')}}{\Delta X^{(\gamma')}} \\ \left(N_B^{(\gamma')} - N_B^{(\beta)} \right) \frac{\mathrm{d}X^{\gamma'|\beta}}{\mathrm{d}t} &= \frac{\tilde{D}^{(\gamma')} \Delta N_B^{(\gamma')}}{\Delta X^{(\gamma')}} - \frac{\tilde{D}^{(\beta)} \Delta N_B^{(\beta)}}{\Delta X^{(\beta)}} \\ \left(N_B^{(\beta)} - 0 \right) \frac{\mathrm{d}X^{\beta|Al}}{\mathrm{d}t} &= \frac{\tilde{D}^{(\beta)} \Delta N_B^{(\beta)}}{\Delta X^{(\beta)}} - 0 \end{aligned} \tag{12}$$

where: $N_B^{(\gamma')}$ denotes the molar fraction of component B in γ' phase; $X^{\gamma|\gamma'}$ denotes the position of the boundary between $\gamma \,|\, \gamma'$ interface; $\Delta X^{(\gamma')}$ is the thickness of the γ' phase and $\Delta N_B^{(\gamma')}$ denotes the difference of concentration in the γ' phase of the component B.

The growth rate of both γ' and β phase can be expressed as the difference in the velocities of the two interfaces:

$$\begin{aligned} \frac{\mathrm{d}\Delta X^{(\gamma')}}{\mathrm{d}t} &= \frac{\mathrm{d}X^{\gamma'|\beta}}{\mathrm{d}t} - \frac{\mathrm{d}X^{\gamma|\gamma'}}{\mathrm{d}t} \\ \frac{\mathrm{d}\Delta X^{(\beta)}}{\mathrm{d}t} &= \frac{\mathrm{d}X^{\beta|Al}}{\mathrm{d}t} - \frac{\mathrm{d}X^{\gamma'|\beta}}{\mathrm{d}t} \end{aligned} \tag{13}$$

By substituting Eq. (12) into (13) finally we obtain:

$$\begin{aligned} \frac{\mathrm{d}\Delta X^{(\gamma')}}{\mathrm{d}t} &= \frac{1}{\left(N_B^{(\gamma')} - N_B^{(\beta)} \right)} \left(\frac{\tilde{D}^{(\gamma')} \Delta N_B^{(\gamma')}}{\Delta X^{(\gamma')}} - \frac{\tilde{D}^{(\beta)} \Delta N_B^{(\beta)}}{\Delta X^{(\beta)}} \right) + \frac{1}{\left(1 - N_B^{(\gamma')} \right)} \frac{\tilde{D}^{(\gamma')} \Delta N_B^{(\gamma')}}{\Delta X^{(\gamma')}} \\ \frac{\mathrm{d}\Delta X^{(\beta)}}{\mathrm{d}t} &= \frac{1}{N_B^{(\beta)}} \frac{\tilde{D}^{(\beta)} \Delta N_B^{(\beta)}}{\Delta X^{(\beta)}} - \frac{1}{\left(N_B^{(\gamma')} - N_B^{(\beta)} \right)} \left(\frac{\tilde{D}^{(\gamma')} \Delta N_B^{(\gamma')}}{\Delta X^{(\gamma')}} - \frac{\tilde{D}^{(\beta)} \Delta N_B^{(\beta)}}{\Delta X^{(\beta)}} \right) \end{aligned} \tag{14}$$

3. Calculations

The calculation of the growth rate of γ' and β phases

TABLE 1

Thermodynamic and kinetic data used to simulate the reactions in the Ni-Al system at 1373 K

Phase	concentration of N_{Ni}	Wagner's interdiffusion coefficient in Ni-Al system, $\tilde{D}^{(\alpha)}$ [cm^2s^{-1}]	Wagner's interdiffusion coefficient in Ni-Al-Hf system, $\tilde{D}^{(\alpha)}$ [cm^2s^{-1}]
$AlNi_3$	0.77-0.725	$2.92\ 10^{-11}$	$2.92\ 10^{-11}$
AlNi	0.625-0.45	$9.15\ 10^{-10}$	$1.82\ 10^{-9}$

need the second derivative of the Gibbs potential (or activity), Eqs. (14) and (11). The activity of the Ni and Al at 1373 K are presented in Figure 1 [21].

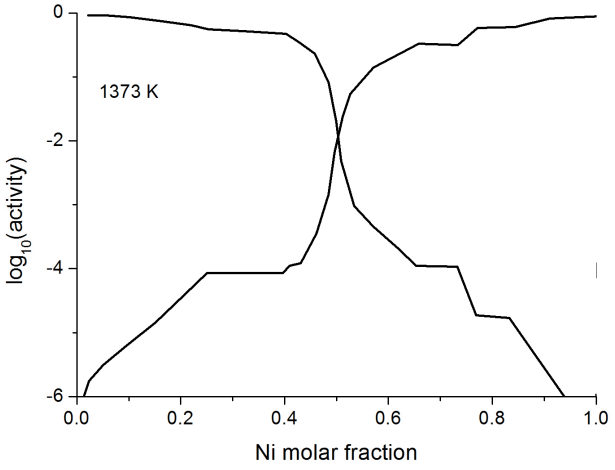

Fig. 1. The Ni and Al activity at 1373 K [21]

According to Campbell [22], Y. Ma, A. J. Ardell [23] and H. Wei at al. [24]it has been assumed that the interdiffusion coefficient in the β-NiAl phase depends on the concentration.

In this work the interdiffusion coefficient $\tilde{D}^{Int}_{NiAl}$ in β-NiAl phase suggested by Campbell [22] was applied. There are several intermetallic phases in the Ni-Al binary system [25, 26]. Two of them (γ'-Ni_3Al and β-NiAl) were considered in this calculation. The data used in simulations are shown in Table 1 [27,28,29].

4. Experimental procedure

The aluminide coatings were deposited using the CVD equipment BPXPR0325S manufactured by the IonBond company (Fig. 3). The aluminizing process was described in details in references [19,30]

The commercial nickel of 99.95 wt. % purity was used in this study. The cylindrical samples of the 20 mm diameter and 4 mm high were cut and grounded up to SiC No 1000, degreased in ethanol and ultrasonically cleaned.

The aluminizing process was performed in two ways. In the first one, the aluminizing process was conducted for 8 or 11 hours at the temperature 1373K. Aluminium chloride vapour (AlCl3) was produced in an external generator according to the reaction: $2Al+6HCl\rightarrow 2AlCl_3+3H_2$. Then the saturating atmosphere was transported in a stream of hydrogen gas into the CVD reactor, where nickel samples were placed. The $AlCl_3$ vapour reacted with the nickel at 1373K and grains of the NiAl phase were formed according to the reaction:

$$2AlCl_3+2Ni+3H_2\rightarrow 2AlNi+6HCl \qquad (15)$$

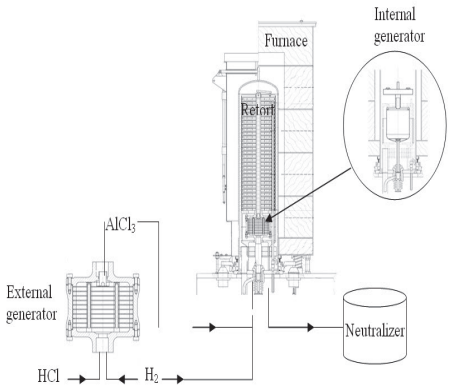

Fig. 2. Scheme of the apparatus of the CVD method

The aluminizing process consisted of the following stages:
I – heating from the room temperature up to 1373 K;
II – aluminizing at 1373 K for 60 minutes;
III – aluminizing for 360 minutes or aluminizing with hafnizing at 1375 K for 360 minutes;
IV– aluminizing at 1375 K for 60 minutes;
V – cooling samples with the furnace.

The aluminide coatings were deposited on pure nickel and on nickel with 3 μm hafnium layer deposited by the EB-PVD method [30-32]. In this method, a material to evaporate (placed in a water-cooled Cu crucible) is melted by the focused high energy electron beam. Power density in the electron beam spot (on the surface of the material) can reach over 40 kW/cm^2 and any material around the spot can be easily evaporated. After the evaporation process, material can be easily evacuated (it does not stick to the crucible). The additional advantage of this method is that the material can have any form (wire, sheet pieces, pellets, etc) and can be easily supplemented in the crucible. For this work Balzers ESQ 110 (four hearts crucible) electron beam evaporator was used. Electrons emitted from a hot tungsten cathode (Fig. 3), are initially focused by the Wehnelt electrode then, are accelerated by the electric field to the anode and achieve energies up to 10 keV. Electron beam is focused and deflected (by an angle of 270º), forming a high energy electron spot on the surface of the material in the crucible. The distance between the evaporating source (crucible) and substrates was 150 mm.

The rate of the material deposition (v) depends on the electron beam power:

$$P_E = U_E \times I_E \qquad (16)$$

where U_E – anode voltage and I_E – electron beam current (cathode emission current).
Deposition rates for Hf were established as follows:
v_{Zr} = 1.0 µm/min for I_E = 310 mA, U_E = 9.5 kV

Technological stages for Hf layers deposition were as follows:

- substrates cleaning in a detergent and placing in a substrates holder
- pumping the chamber to p = 2× 10^{-6} hPa
- substrate heating to 300 ºC (t_H = 20 min)
- evaporation of the Hf layer with the deposition rate (v) mentioned in order to obtain the proper coating thickness (evaporation time t_E = 50 s)
- crucible rotation (changing the position to another material)
- cooling substrates to 50 ºC (about 1 hour)
- venting the chamber.

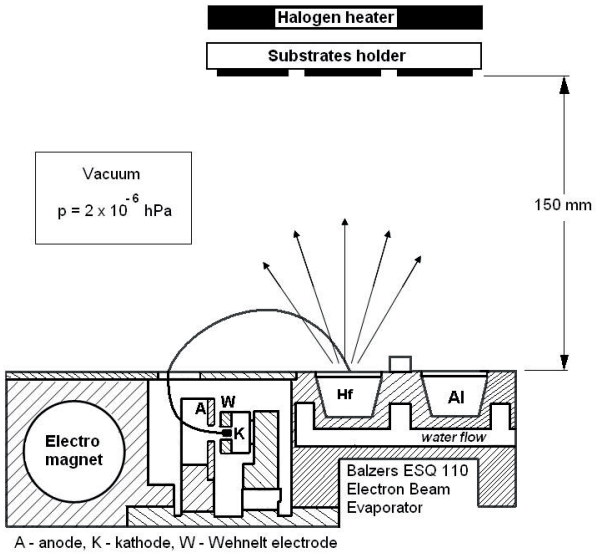

Fig. 3. Scheme of the apparatus of the EB-PVD method

5. Results

The microstructure of the cross-section of coatings was investigated by an optical microscope Nikon Epiphot 300, a scanning electron microscope (SEM) Hitachi S-3400N and an energy dispersive spectroscope (EDS).

a) b)

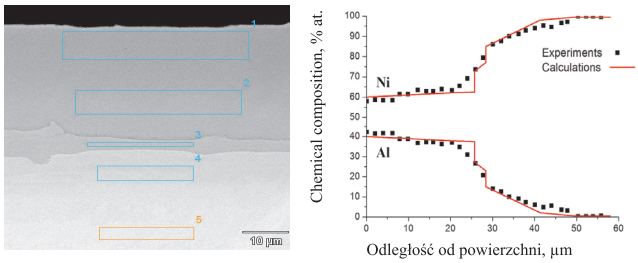

Figure 4. The microstructure (a) and chemical composition on the cross-section (b) of a non-modified aluminide coating deposited for 8 hours by the CVD method on pure nickel

TABLE 2
Chemical composition on the cross-section of a non-modified aluminide coating deposited for 8 hours by the CVD method on pure nickel

Point	Chemical composition, % at	
	Al	Ni
1	39.28	60.72
2	37.60	62.40
3	20.84	79.16
4	8.94	91.06
5	-	100

The SEM investigation and the EDS analysis of the aluminide coating on pure nickel revealed its triple-zone structure (Fig. 4, Table 2). In the first zone, on the top of the coating, the proportion of Ni do Al corresponds to the β-NiAl phase (Table 2, Point 1, 2). The thickness of the top-zone is about 20 µm. The second zone, below, is thinner (about 5 mm) and consists of the γ'-Ni_3Al phase (Table 2, Point 3) The chemical composition of the third, inner zone, corresponds to the γ-Ni(Al) phase, that is the aluminum solid solution in nickel (Table 2, Point 4). The chemical composition of the zone below the γ-Ni(Al) phase is the same as the matrix composition that is pure nickel (Table 2, Point 5).

The microstructure of the coating deposited by both EB-PVD and CVD methods is presented in Figure 5. The β-NiAl phase forms a top layer of the coating, which is 30 µm thick, and the γ'-Ni_3Al phase is situated below, like in the previous case presented in Figure 4. Approximately 5 µm thick phase enriched with hafnium is formed below, on the sample's surface.

a) b)

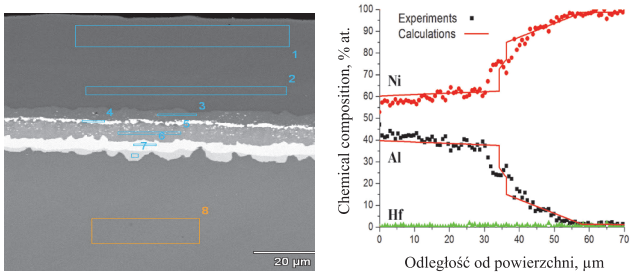

Fig. 5. Microstructure (a) and the EDS linear analysis (b) on the cross-section of the aluminide coating deposited for 8 hours on the nickel sample with 3 mm thick hafnium layer

TABLE 3
Chemical composition on the cross-section of the aluminide coating deposited for 8 hours on the nickel sample with 3 mm thick hafnium layer

Point	Chemical composition, % at		
	Al	Ni	Hf
1	40.26	59.42	0.32
2	37.38	62.36	0.26
3	31.03	68.43	0.55
4	26.44	71.26	2.30
5	20.07	70.51	9.42
6	18.18	74.41	7.41
7	4.18	75.37	20.45
8	1.09	98.29	0.62

a) b)

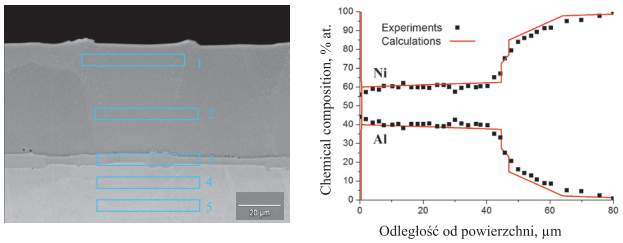

Fig. 6. Microstructure (a) and the EDS linear analysis (b) on the cross-section of the hafnium doped aluminide coating deposited for 11 hours on the nickel sample by the CVD method

TABLE 4

Chemical composition on the cross-section of the hafnium doped aluminide coating deposited for 11 hours on the nickel substrate

Point	Chemical composition, % at		
	Al	Ni	Hf
1	37.38	60.72	1.9
2	36.60	62.40	1.0
3	20.80	79.20	-
4	8.90	91.1	-
5	-	100	-

The microstructure of the hafnium doped aluminide coating deposited by the CVD method is similar to the undoped aluminide coating (see Figure 4) and consists of the same phases. What is more, the thickness of the γ'-Ni_3Al phase is the same – 5 µm, whereas the thickness of the β-NiAl phase is 40 µm. Hafnium has not been detected. It may be assumed, that its content is very low and it has dissolved in the coating or formed inclusions too small to be detected by the SEM technique, like zirconium [30].

The calculations' results of the reactive diffusion between Ni and Al as well as the experimental data of the thickness of different phases are presented in Figure 6. Hafnium addition accelerates the growth of the β-NiAl phase, whereas the thickness of the γ'-Ni_3Al phase remains the same.

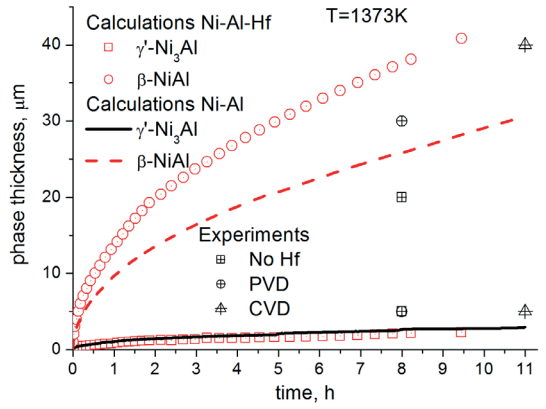

Fig. 7. The kinetic of the phase formation in Ni-Al-Hf system at 1373 K

In all three coatings, deposited in these research, the thickness of the γ'-Ni_3Al phase is the same, but the thickness of the β-NiAl phase is different. Both hafnium addition and the elongation of the deposition time (from 8 to 11 h) influences the growth of the β-NiAl phase, while the thickness of the γ'-Ni_3Al phase remains the same. The experimental results are similar to the calculated values.

6. Summary

The diffusion between γ-Ni| γ'-Ni_3Al and γ'-Ni_3Al|β-NiAl interfaces has been calculated. The generalized Darken method was used. The method deals with the Wagners integral diffusion coefficients and activities of the components. The obtained results (see Figure 7) well describe the process of hafnium doped and undoped aluminide coatings formation well. Aluminide coatings were deposited by the CVD method, whereas hafnium was co-deposited with aluminium in the CVD process or a hafnium layer was deposited by the EB-PVD method prior to the CVD process. In all cases experimental results agree with the simulation. Hafnium behaves as a marker and does not take part in the diffusion process and does not influence neither chemical nor phase composition of the coating, but it accelerates the growth of the β-NiAl phase.

Acknowledgment:

The presented research was supported by the National Science Centre, Poland, project number 2011/01/B/ST8/05036

REFERENCES:

[1] G.W. Goward, Materials Science and Technology **2**, 194-200 (1986).
[2] Y. Tamarin, Protective Coatings for Turbine Blades, AMS International, Materials Park, 2002.
[3] B.A. Pint, J.R. Di Stefano, I.G. Wright, Materials Science and Engineering A **415**, 255-263 (2006).
[4] Loira E. Intermetallics **8**, 1339-1345 (2000).
[5] Loira E. Intermetallics **9**, 997-1001 (2001).
[6] Z. Zhang, J.A. Havnes, G. Wright, B.A. Pint, K.M. Cooley, W.Y. Lee, P.K. Liaw, Metall. Mater. Trans A. Phys. Metall. Mater. Sci. **32**, 1727-1741 (2001).
[7] M. Zagula-Yavorska J. Sieniawski, JMEPEG **23**, 918-926 (2014).
[8] M. Zagula-Yavorska, J. Sieniawski, T. Gancarczyk, Archives of Metallurgy and Materials **57**, 503-509 (2012).
[9] D. Li, H. Guo, D. Wang, T. Zhang, S. Gong, H. Xue, Cyclic Corrosion Science **66**, 125-135 (2013).
[10] G.H. Hwang, J.W. Choi, S. Kang, Z. Metallkd. **96**, 269-275 (2005).
[11] Y. Wang, M. Suneson, G. Sayre, Surf .Coat. Technol. **206**, 1218-1228 (2011).
[12] D. Li, H. Guo, D. Wang, T. Zhang, S. Gong, X.Hubin, Corr. Sci. **66**, 125-135 (2013).
[13] A.H. Heuerw, D.B. Hovis, J.L. Smiałek, B. Gleson, Journal of American Ceramic Society **94**, 146-153 (2011).
[14] B.A. Pint, K.L. More, P.F. Tortoreli, Mater. Sci. Forum **1**, 411-418 (2001).
[15] B.A Pint, K.L More, I.G. Wright, Oxid. Met. **59**, 257-283

(2003).
[16] J.P. Stacy, Y. Zhang, B.A. Pint, J.A. Haynes, B.T. Hazel, B.A. Nagaraj, Surf. Coat. Technol. **202**, 632-636 (2007).
[17] Y. Wang, M. Suneson, G. Sayre, Surf. Coat. Technol. **206**, 1218-1228 (2011).
[18] J. Romanowska, M. Zagula-Yavorska, J. Sieniawski, Bull. Mater. Sci. **36**, 1043-1048 (2013).
[19] M. Yavorska, J. Sieniawski, M. Zielińska, Archives of Metallurgy and Materials **56**, 187-192 (2011).
[20] C. Wagner, Acta Metallurgica, **17**, 99-107 (1969).
[21] W. Huang, Y.A. Chang, Intermetallics **6**, 487-498 (1998).
[22] C.E. Campbell, Acta Mat. **56**, 4277-4290 (2008).
[23] Y. Ma, A.J. Ardell, Mat. Sci. & Eng. A **516**, 259-262 (2008).
[24] H. Wei, X. Sun, Q. Zheng, G. Hou, H. Guan , Z. Hu, J. Mater. Sci. Technol. **20**, 196-198 (2004).
[25] I. Ansara, N. Dupin, H. L. Lukas , B. Sundman, J. of Alloys and Comp. **247**, 20-30 (1997).
[26] FactSage metal alloy databases (www.csct.polymtl.ca).
[27] R.E. Hoffman, F. W. Pikus, R. A. Ward, Trans. AIME **206**, 483-492 (1956).
[28] T.S. Lundy, J.F. Murdock, J. Appl. Phys. **33**, 1671-1678 (1962).
[29] J.R. MacEwan, J.U. MacEwan, L. Yaffe, Can. J. Chem. **37**, 1623-1628 (1959).
[30] M. Zagula-Yavorska, J. Morgiel, J. Romanowska, J. Sieniawski, Materials Letters, **139**, 50-54 (2015).
[31] B. Wierzba, J. Romanowska, M. Zagula-Yavorska, J. Markowski, J. Sieniawski, High Temperature Materials and Processes, **5**, 495-502 (2015).
[32] J. Romanowska, M. Zagula-Yavorska, J. Sieniawski, J. Markowski, Open Journal of Metal, **3**, 92-99 (2013).